Langmuir
Article

pubs.acs.org/Langmuir

Hierarchically Nanostructured Barium Sulfate Fibers

Issis C. Romero-Ibarra,[†] Geonel Rodríguez-Gattorno,[‡] Mario F. García-Sánchez,[†] Antonio Sánchez-Solís,[†] and Octavio Manero*,[†]

[†]*Instituto de Investigaciones en Materiales, Universidad Nacional Autónoma de México, Ciudad Universitaria, Coyoacán 04510, México D.F., México and* [‡]*Centro de Investigación en Ciencia Aplicada y Tecnología Avanzada, Instituto Politécnico Nacional; Irrigación 11500, México D.F., México*

Received November 4, 2009. Revised Manuscript Received December 12, 2009

$BaSO_4$ nanostructures with controlled morphologies were successfully produced via one-step process through precipitation of $BaSO_4$ in aqueous and organic media. The synthesis is carried out by mixing solutions of $BaCl_2$ and Na_2SO_4 in presence of EDTA (disodium ethylenediaminetetraacetic acid) at room temperature. The influence of the reaction conditions such as initial reactants concentration, pH, EDTA/[Ba^{2+}] ratio and aging on the $BaSO_4$ nanoparticles organization is studied. Using EDTA in aqueous media, spherical secondary particles of 500 nm diameter are obtained, which are formed by 4 nm size primary particles. With dimethyl sulfoxide and small amounts of water (5%) and EDTA, the aging process allows the production of long homogeneous fibers, related to hierarchical organization of $BaSO_4$ nanoparticles. Direct observation of self-assembling of primary particles by HRTEM allows proposing a mechanism for fiber formation, which is based on multipolar attractions that lead to a brick-by-brick organization along a preferential orientation. Results evidence the role of EDTA as controlling agent of the morphology and primary and secondary mean particle size.

Introduction

The bioinspired mineralization synthesis strategy allows the controlled and reproducible production of complex materials with specific size, shape, composition and hierarchical organization.[1−7] The hierarchical organization of nanoparticles, from homogeneous colloidal crystallization to the directed self-assembly of colloidal particles, is promoted by covalent and noncovalent interactions.[8] The particle-based crystallization mechanisms (involving mesoscopic transformations of nanoparticles precursor phase) are usually named "oriented attachment" and "mesocrystal formation". Oriented attachment involves the directed attachment of oriented primary building block particles under subsequent crystallographic fusion, which usually leads to one-dimensional nanomaterials.[9,10] This process involves the spontaneous self-organization of the nanobuilding blocks and its subsequent coalescence.[3,11−15] Mesocrystals, on the other hand, are colloidal crystals composed of crystalline nanoparticles in a perfect three-dimensional crystallographic array, so they scatter light like a single crystal, although they are formed by nanoparticle superstructures.[2] A brick-by-brick particle interactions have been previously suggested as a self-assembly formation mechanism.[2]

Barium sulfate ($BaSO_4$) has an industrial relevance due to its whiteness, inertness, high specific gravity and optical properties, such as opacity to UV and X-rays radiation.[16−19] It is mainly used as a radio-contrast agent, filler in plastics, extender in paints, coatings and additive in pharmaceutical products and in printing ink.[1,16,18,20−25] Nowadays, interest in this material has been renewed with the development of methods to produce nanosize particles, supraparticles of a well-controlled number of nanoparticles and mesocrystals that mimic biomineralization processes.[2] Among the methods for nanoparticle synthesis, controlled precipitation has the advantage of good reproducibility, low-cost and the use of mild reaction conditions within a relatively simple process.[13,26] This method can improve the quality of the product in terms of controlling the particle size and the particle size

*Corresponding author. Telephone: (+525) 5622 4576, (+525) 5622 4589. Fax: (+525) 5616 1201. E-mail: manero@servidor.unam.mx.

(1) Niemann, B.; Veit, P.; Sundmacher, K. *Langmuir* **2008**, *24*, 4320–4328.
(2) Xu, A.-W.; Ma, Y.; Cölfen, H. *J. Mater. Chem.* **2007**, *17*, 415–449.
(3) Yu, S.-H.; Cölfen, H. *J. Mater. Chem.* **2004**, *14*, 2124–2147.
(4) Wang, T.; Cölfen, H. *Langmuir* **2006**, *22*, 8975–8985.
(5) Wang, T.; Reinecke, A.; Cölfen, H. *Langmuir* **2006**, *22*, 8986–8994.
(6) Liu, B.; Zeng, H. C. *Langmuir* **2004**, *20*, 4196–4204.
(7) Grzelczak, M.; Perez-Juste, J.; Mulvaney, P.; Liz-Marzan, L. M. *Chem. Soc. Rev.* **2008**, *37*, 1783–1791.
(8) Edwards, E. W.; Wang, D.; Möhwald, H. *Macromol. Chem. Phys.* **2007**, *208*, 439–445.
(9) Penn, R. L.; Banfield, J. F. *Geochim. Cosmochim. Acta* **1999**, *63*, 1549–1557.
(10) Ratkovich, A. S.; Penn, R. L. *J. Solid State Chem.* **2008**, *181*, 1600–1608.
(11) Li, B.; Xie, Y.; Jing, M.; Rong, G.; Tang, Y.; Zhang, G. *Langmuir* **2006**, *22*, 9380–9385.
(12) Li, M.; Mann, S. *Langmuir* **2000**, *16*, 7088–7094.
(13) Yu, S.-H.; Antonietti, M.; Cölfen, H.; Hartmann, J. *Nano Lett.* **2003**, *3*, 379–382.
(14) Zhang, H.; Liu, Y.; Zhang, J.; Sun, H.; Wu, J.; Yang, B. *Langmuir* **2008**, *24*, 12730–12733.
(15) Ribeiro, C.; Vila, C.; Stroppa, D. B.; Mastelaro, V. R.; Bettini, J.; Longo, E.; Leite, E. R. *J. Phys. Chem. C* **2007**, *111*, 5871–5875.
(16) Bala, H.; Fu, W.; Guo, Y.; Zhao, J.; Jiang, Y.; Ding, X.; Yu, K.; Li, M.; Wang, Z. *Colloids Surf. A* **2006**, *274*, 71–76.
(17) Fenter, P.; McBride, M. T.; Srajer, G.; Sturchio, N. C.; Bosbach, D. *J. Phys. Chem. B* **2001**, *105*, 8112–8119.
(18) Nagaraja, B. M.; Abimanyu, H.; Jung, K. D.; Yoo, K. S. *J. Colloid Interface Sci.* **2007**, *316*, 645–651.
(19) Nuutinen, J. P.; Clerc, C.; Törmälä, P. *J. Biomater. Sci., Polym. Ed.* **2003**, *14*, 665–676.
(20) Stražar, K.; Kavčič, M.; Simčič, J.; Pelicon, P.; Šmit, Ž.; Kump, P.; Jaćimović, R.; Antolič, V.; Cör, A. *Nucl. Instrum. Methods Phys. Res., Sect. B* **2006**, *249*, 719–722.
(21) Wu, G.; Zhou, H.; Zhu, S. *Mater. Lett.* **2007**, *61*, 168–170.
(22) Uchida, M.; Sue, A.; Yoshioka, T.; Okuwaki, A. *CrystEngComm* **2001**, *3*, 21–26.
(23) Kieffer, R.; Mangin, D.; Puel, F.; Charcosset, C. *Chem. Eng. Sci.* **2009**, *64*, 1885–1891.
(24) Kieffer, R.; Mangin, D.; Puel, F.; Charcosset, C. *Chem. Eng. Sci.* **2009**, *64*, 1759–1767.
(25) Cafiero, L. M.; Baffi, G.; Chianese, A.; Jachuck, R. J. J. *Ind. Eng. Chem. Res.* **2002**, *41*, 5240–5246.
(26) Rodriguez-Gattorno, G.; Diaz, D.; Rendon, L.; Hernandez-Segura, G. O. *J. Phys. Chem. B* **2002**, *106*, 2482–2487.

distribution (PSD).[27−33] The concentration, pH, temperature, reaction media[12,34−36] and the introduction of stabilizing agents (chelating agents,[37] polymeric inhibitors,[38−40] surfactants,[1,14,35,41] and other organic additives,[2−4,16,18,21,28,30,31,34,37,41−43]) are the most important parameters to promote nucleation and controlled growth.[44−46]

The control of shapes of $BaSO_4$ has been the object of numerous studies.[1,2,4,5,12,13,22,25,27,31,32,34−39,41,47−54] Li et al. prepared ellipsoidal nanocrystals by using ethylenediaminetetraacetic acid (EDTA),[37] while Yu et al. obtained fibers in presence of sodium polyacrylate.[13] Likewise, using the same agent, Wang et al. have reported a well-established method to obtain cones, fiber bundles as well as elucidating their crystallization[5] and its associated kinetic mechanisms.[4] The kinetics of the crystallization process involves the nucleation and growth rates of the crystal, which are directly dependent on the saturation ratio. This ratio is the driving force for nucleation and growth and determines the induction period along which a stationary cluster distribution is reached and critical nuclei are formed.[30] Judat and Kind proposed a mechanism for $BaSO_4$ formation that involves molecular and aggregative growth.[55] These mechanisms can also lead to inclusions and to a porous internal crystal structure by molecular crystal growth, i.e., by incorporation of monomers into the crystal. Qi et al. synthesized a variety of well-defined morphologies using double-hydrophilic block copolymers as crystal growth modifiers to direct the controlled precipitation as a function of pH.[56,57] A possible mechanism for the development of (defect-free growth) bundles of $BaSO_4$ nanofilaments from the amorphous precursor particles by attractive van der Waals forces and crystal multipole forces is proposed.[58] The alignment of assembled nanoparticles is inferred from the external shape of the structures, but direct observations of nanostructures were not reported. In general, the supraparticle chemistry involved in this process is now a very rapidly developing research field inspired in materials found in nature. Up to now, details related to the perfect alignment of nanoparticles in building units that form mesocrystals remains unclear.

In the present work, the morphology of $BaSO_4$ nanostructures, synthesized by controlled precipitation, is studied in detail. The influence of the capping agent, pH, reaction media and aging on the agglomerate shape and primary and secondary particle size is further analyzed. The synthesis of nanometric $BaSO_4$ in dimethyl sulfoxide (DMSO) allows the production of long fibers. HRTEM observations allowed a direct assessment of self-assembled primary barium sulfate nanoparticles, which suggest a brick-by-brick assembling mechanism via hierarchical organization during the aging processes.

Experimental Section

Materials. The following analytical reagents were used as received: $BaCl_2 \cdot 2H_2O$ (Baker, 99.9%), Na_2SO_4 (Baker, 99%), disodium ethylenediaminetetraacetic acid (EDTA) EDTA−2Na·$2H_2O$ (Baker, 99.9%), and dimethyl sulfoxide (DMSO) $(CH_3)_2S{=}O$ (Aldrich, 99.9%).

Precipitation Procedure in Aqueous Media: $BaSO_4$ Aggregates in the Presence of EDTA. A 100 mL sample of 0.1 M $BaCl_2$ was added to 100 mL of 0.1 M EDTA−2Na·$2H_2O$ under vigorous magnetic stirring at room temperature. Various EDTA concentrations were considered (0.05, 0.01, and 0.001 M) and the pH was adjusted from 4 to 8 using HCl. Thereafter, 100 mL of 0.1 M Na_2SO_4 was added. The resulting suspension was collected; the precipitates of $BaSO_4$ were separated from the mother liquor by decantation and washed with distilled water several times. After the centrifugation process, the particles were dried in an oven at 110 °C for 24 h. The product was ground up for analysis.

Precipitation Procedure in Organic Media: $BaSO_4$ Aggregates/DMSO in Presence of EDTA. The DMSO was dried for 16 h with previously activated Linde 4 Å sieves at 500 °C.[59] A 2.19 g sample of $BaCl_2$ was dissolved in 200 mL of DMSO. Simultaneously, 3.21 g of EDTA−2Na·$2H_2O$ was dissolved in 200 mL of DMSO at 60 °C under strong magnetic stirring for 30 min. Thereafter, both solutions were mixed and 1.42 g of Na_2SO_4 was added with magnetic stirring. The synthesis was carried out under inert atmosphere. The solvent was eliminated and the precipitated particles were dried in the oven with vacuum at 110 °C for 24 h.

Preparation in DMSO/H_2O in Presence of EDTA. A 5 vol % aliquot of water was added, following an analogous preparation procedure mentioned above.

In the synthesis stage, samples were allowed to age in solution.

Structural Characterization. *X-ray Diffraction (XRD).* XRD patterns were obtained in a Bruker AXSD8 advanced diffractometer (Cu Kα radiation, λ = 1.54184 Å at 35 kV and 30 μA with a scanning speed of 1° 2θ/min).

Electron Microscopy. Scanning electron microscopy (SEM) studies were carried out in a Leica Stereoscan Scanning -440. The samples were gold-coated using a fine-coat ion sputter, Jeol JFC-110.

High-resolution transmission electron microscopy (HRTEM) studies were carried out in a Jeol 4000EX at 400 kV. Samples were prepared by evaporation of a drop of the aqueous suspension on an amorphous carbon-coated Cu TEM grid. The size distribution was estimated by particle analysis of at least 100 particles in the TEM images. The morphology analysis of $BaSO_4$ fibers was effected using a SHAPE program version 7.1.2 based on simple

(27) Burda, C.; Chen, X.; Narayanan, R.; El-Sayed, M. A. *Chem. Rev.* **2005**, *105*, 1025–1102.
(28) Niemann, B.; Sundmacher, K. *Chem. Eng. J.* **2008**, *143*, 314–325.
(29) Öncül, A. A.; Niemann, B.; Sundmacher, K.; Thévenin, D. *Chem. Eng. J.* **2008**, *138*, 498–509.
(30) Öncül, A. A.; Sundmacher, K.; Seidel-Morgenstern, A.; Thévenin, D. *Chem. Eng. Sci.* **2006**, *61*, 652–664.
(31) Schwarzer, H.-C.; Peukert, W. *Chem. Eng. Technol.* **2002**, *25*, 657–661.
(32) Sugimoto, T. *Adv. Colloid Interface Sci.* **1987**, *28*, 65–108.
(33) Zhu, C. *Geochim. Cosmochim. Acta* **2004**, *68*, 3327–3337.
(34) La Mer, V. K.; Dinegar, R. H. *J. Am. Chem. Soc.* **1950**, *72*, 4847–4854.
(35) La Mer, V. K.; Dinegar, R. H. *J. Am. Chem. Soc.* **1951**, *73*, 380–385.
(36) Nielsen, A. E. *Acta Chem. Scand.* **1961**, *15*, 441–442.
(37) Li, J.; Xu, Y.; Wu, D.; Sun, Y. *China Particuology* **2003**, *1*, 134–136.
(38) Black, S. N.; Bromley, L. A.; Cottier, D.; Davey, R. J.; Dobbs, B.; Rout, J. E. *J. Chem. Soc., Faraday Trans.* **1991**, *87*, 3409–3414.
(39) Xiao, J.; Kan, A. T.; Tomson, M. B. *Langmuir* **2001**, *17*, 4668–4673.
(40) Zhao, X.; Yu, J.; Tang, H.; Lin, J. *J. Colloid Interface Sci.* **2007**, *311*, 89–93.
(41) Bokern, D. G.; Ducker, W. A.; Hunter, K. A.; McGrath, K. M. *Colloids Surf. A* **2003**, *229*, 43–53.
(42) Qi, L.; Ma, J.; Cheng, H.; Zhao, Z. *Colloids Surf. A* **1996**, *108*, 117–126.
(43) Li, M.; Schnablegger, H.; Mann, S. *Nature* **1999**, *402*, 393–395.
(44) Jones, F.; Oliveira, A.; Rohl, A. L.; Ogden, M. I.; Parkinson, G. M. *CrystEngComm* **2006**, *8*, 869–876.
(45) Su, Y.-F.; Kim, H.; Kovenklioglu, S.; Lee, W. Y. *J. Solid State Chem.* **2007**, *180*, 2625–2629.
(46) Boerlage, S. F. E.; Kennedy, M. D.; Bremere, I.; Witkamp, G. J.; van der Hoek, J. P.; Schippers, J. C. *J. Membr. Sci.* **2000**, *179*, 53–68.
(47) Chen, J.; Zheng, C.; Chen, G. A. *Chem. Eng. Sci.* **1996**, *51*, 1957–1966.
(48) Guo, Z.; Jones, A. G.; Li, N. *Chem. Eng. Sci.* **2006**, *61*, 1617–1626.
(49) Song, X.; Sun, S.; Fan, W.; Yin, Z. *Mater. Lett.* **2003**, *57*, 3026–3030.
(50) Wang, F.; Xu, G.; Zhang, Z.; Xin, X. *Colloids Surf. A* **2005**, *259*, 151–154.
(51) Zhiqian, J.; Zhongzhou, L. *J. Membr. Sci.* **2002**, *209*, 153–161.
(52) Murdaugh, A. E.; Liddelow, M.; Schmidt, A. M.; Manne, S. *Langmuir* **2007**, *23*, 5852–5856.
(53) Murdaugh, A. E.; Manne, S. *Langmuir* **2009**, *25*, 9792–9796.
(54) Roelands, C. P. M.; Roestenberg, R. R. W.; ter Horst, J. H.; Kramer, H. J. M.; Jansens, P. J. *Cryst. Growth Des.* **2004**, *4*, 921–928.
(55) Judat, B.; Kind, M. *J. Colloid Interface Sci.* **2004**, *269*, 341–353.
(56) Qi, L.; Cölfen, H.; Antonietti, M. *Angew. Chem., Int. Ed.* **2000**, *39*, 604–607.
(57) Qi, L.; Cölfen, H.; Antonietti, M. *Chem. Mater.* **2000**, *12*, 2392–2403.
(58) Qi, L.; Cölfen, H.; Antonietti, M.; Li, M.; Hopwood, J. D.; Ashley, A. J.; Mann, S. *Chem.—Eur. J.* **2001**, *7*, 3526–3532.
(59) Kissing, P.; Heineman, W. *Laboratory Techniques in Electroanalytical Chemistry*. Marcel Dekker: New York, 1984.

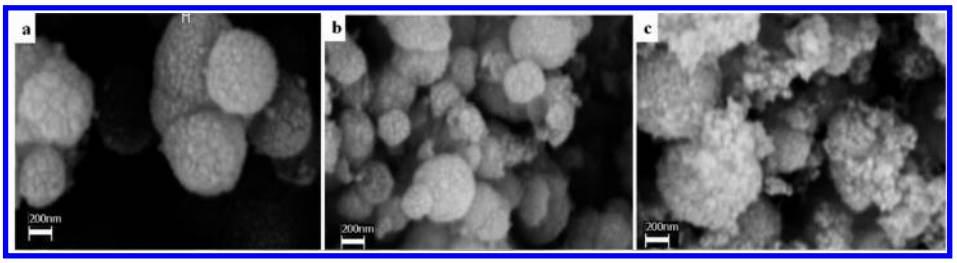

Figure 1. Selected SEM images of $BaSO_4$ aggregates obtained in aqueous media/EDTA [0.1 M]: (a) pH = 4, (b) pH = 7, and (c) pH = 8.

geometric considerations according to the Bravais−Friedel−Donnay−Harker (BFDH) methodology.[60−62]

Results and Discussion

X-ray diffraction (XRD) patterns (Supporting Information Figure S1) show that in general, all $BaSO_4$ samples crystallized in an orthorhombic structure (JCPDS No. 24−1035) and second phases are not present. The lattice parameters (*a*, *b*, and *c*) calculated from the average peaks positions are as follows: $a = 0.7152 \pm 0.0015$ nm, $b = 0.8885 \pm 0.0033$ nm, and $c = 0.5448 \pm 0.0013$ nm, in coincidence with the reported values.[16,63] The average crystallite size (*D*) was estimated from the XRD patterns (021) peak using the Scherrer formula corrected for the instrument contribution, as follows:

$$D = \frac{0.9\lambda}{\beta \cos \Theta_B} \quad (1)$$

Here, λ is the wavelength of the incident beam, β is the half-peak width of the *hkl* line, and Θ_B is the Bragg diffraction angle. The crystallite sizes obtained are about 4 nm for spherical agglomerates and 12 nm for fibres.

Synthesis in the Presence of EDTA: Influence of pH. SEM micrographs of $BaSO_4$ obtained at different pH values in presence of EDTA are shown in Figure 1. At pH = 4 (Figure 1a) spherical agglomerates of around 500 nm can be observed. An increase of pH from 4 to 7 leads to decreasing size of the agglomerates and the distribution of secondary particle size is less homogeneous (Figure 1b). With further increase of pH, the agglomerate spherical shape is lost (Figure 1c).

The synthesis of $BaSO_4$ in aqueous media in presence of EDTA involves the following reactions:

$$2Cl^-_{(ac)} + Ba^{2+}_{(ac)} + EDTA^{4-}_{(ac)} + 2Na^+_{(ac)} + 2H^+_{(ac)} \leftrightarrows [Ba{-}EDTA]^{2-}_{(ac)} + 2Na^+_{(ac)} + 2Cl^-_{(ac)} + 2H^+_{(ac)} \quad (1)$$

$$EDTA^{4-} + {}_jH^+ \leftrightarrows H_jEDTA^{4-j} \quad (1a)$$

$$[Ba{-}EDTA]^{2-} + H^+ \leftrightarrows [BaHEDTA]^- \quad (1b)$$

$$Ba{-}EDTA'_{(ac)} + SO4^{2-}{}_{(ac)} + 2Na^+_{(ac)} \leftrightarrows BaSO_{4(s)}\downarrow + EDTA'_{(ac)} + 2Na^+_{(ac)} \quad (2)$$

In reaction 1 barium chloride and disodium EDTA yield the $[Ba{-}EDTA]^{2-}$ complex. Reactions 1a and 1b show the fact that complex formation depends on pH and hence $BaSO_4$ yielding is affected in 2. Ba−EDTA′ and EDTA′ denote all possible intermediate complex species. It is important to point out that the initial EDTA concentration is quite important for $BaSO_4$ yielding 2, because it is involved in the precursor concentrations, which in turn affects the nucleation and growth processes.

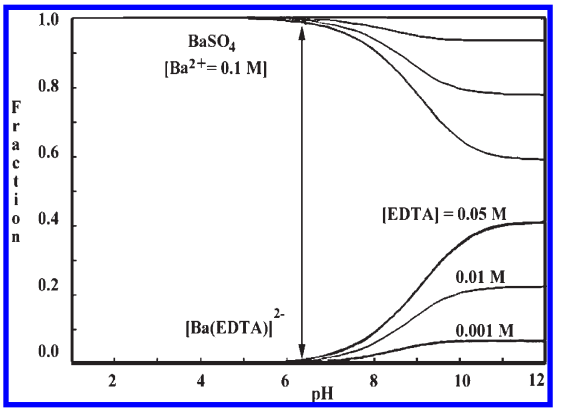

Figure 2. Calculated fraction diagram of the $[Ba{-}EDTA]^{2-}$ complex and $BaSO_{4(s)}$ as functions of pH for various EDTA concentrations.

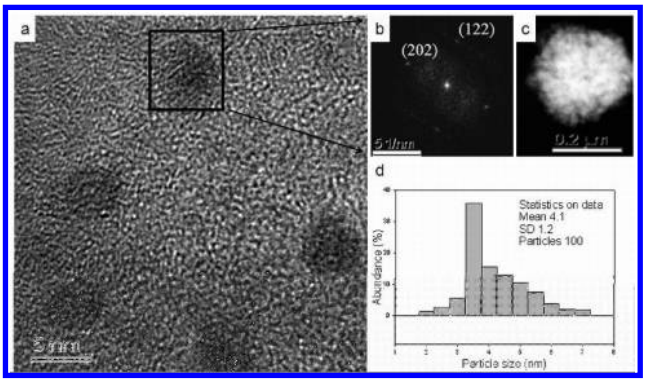

Figure 3. TEM images of $BaSO_4$ aggregates. (a) High-magnification HRTEM image of the $BaSO_4$ clusters, (b) FFT analysis of a nanocrystal, (c) HAADF image showing a spherical agglomerate, and (d) particle size distribution histogram.

In Figure 1, the size of the secondary particles is less uniform for high pH, with departures from the spherical shape. This behavior is expected since, at higher pH, EDTA dissociates more and favors the availability of negatively charge moieties for surface absorption, which in turns increase the interparticle repulsions (see Figure 2). Figure 2 shows a calculated fraction diagram,[64] illustrating the trends of solid $BaSO_4$ and $[Ba{-}EDTA]^{2-}$ complex fractions as functions of pH. It can be noted that, according to the thermodynamics of the system, and only for pH values higher than 6.5, $BaSO_4$ is partially dissolved by complex formation. The inconvenience of $BaSO_4$ synthesis at

(60) Bravais, A. *Etudes Crystallographiques*; Academie des Science: Paris, 1913.
(61) Donnay, J. D. H.; Harker, D. *Am. Mineral.* **1937**, *22*, 446–467.
(62) Friedel, G. *Bull Soc. Fr. Miner.* **1907**, *30*, 326.
(63) Miyake, M.; Minato, I.; Morikawa, H.; Iwai, S.-I. *Am. Mineral.* **1978**, *63*, 506–510.
(64) IUPAC Stability Constant Database, software version 5.7.

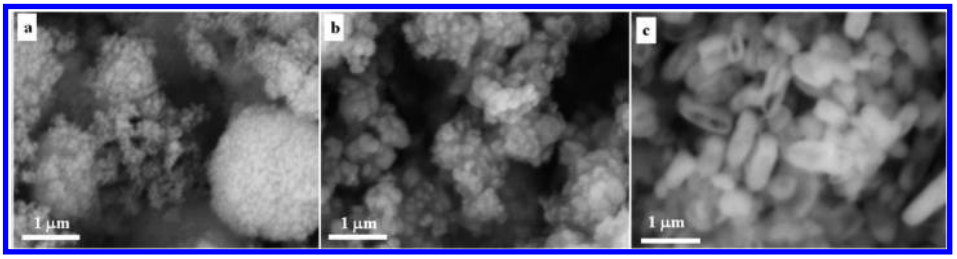

Figure 4. SEM images of $BaSO_4$ aggregates in aqueous media at pH = 4 and for various EDTA concentrations: (a) 0.05 M, (b) 0.01 M, and (c) 0.001 M.

basic pH is that a substantial Ba^{2+} fraction remains soluble with the $[Ba-EDTA]^{2-}$ complex, affecting the reaction yield.

The morphology and size distribution of the primary particles at pH = 4 observed by HRTEM are shown in Figure 3. Dark field images in Figure 3c show roughly spherical agglomerates, in agreement with sizes observed by SEM.

At higher magnifications, crystalline nanoparticles can be observed in the agglomerate (see Figure 3, parts a and d). They have a mean particle size of 4.1 nm ±1.2 nm, in agreement with the particle size estimated from the XRD patterns. The nanocrystals show smooth surfaces and not an elongated morphology. The local fast Fourier transform (FFT) analysis (Figure 3b) shows the equivalent reflections expected for $BaSO_4$.

Synthesis in the Presence of EDTA: The Influence of EDTA Concentration. Because of the reactant equilibria of Ba^{2+} and EDTA species, which strongly affect the supersaturation, the pH level was fixed to study the influence of EDTA concentration.

Figure 4 shows the effect of decreasing EDTA concentration on the morphology of $BaSO_4$ at fixed pH (pH = 4) and at room temperature. For 0.05 M EDTA, and molar ratio $[Ba^{2+}/EDTA]$ of 1:0.5, agglomerate formation is nonuniform with increasing size (compare Figures 1a and 4a). The agglomerate size distribution becomes broader and the spherical shape is lost. This trend continues and becomes more evident for an EDTA concentration of 0.01 M (Figure 4b), $[Ba^{2+}/EDTA]$ = 1:0.1. However, in this case, the spherical form of the primary particles is preserved. At an EDTA concentration of 0.001 M, $[Ba^{2+}/EDTA]$ = 1:0.01, the clusters exhibits a disk-like morphology. For the same conditions, but without EDTA, particle morphology is very similar to that exhibited by samples prepared at lower EDTA concentrations (0.001 M) (Figure 5).

Figure 5 shows the morphology of $BaSO_4$ prepared without EDTA at pH = 4. SEM images (Figure 5a) show the presence of particles having rod-like morphology with broader particle size distribution. The HRTEM study (Figure 5b–d) reveals that these agglomerates consist of monocrystalline particles of around 200 × 400 nm, elongated along the [010] direction. These results and the behavior observed at various pH values are clear evidence of the EDTA stabilizing role in obtaining small particles.

It is important to note that in Figure 2 it is shown that EDTA remains not dissociated at pH = 4, although the results shown in Figure 4 and 5 clearly demonstrate its role as capping agent. Consequently, the EDTA concentration determines not only the morphology, but also the primary and secondary mean particle size and PSD.

All previous samples were allowed to age for more than a week, and SEM micrographs (not shown here) show a slight increase in particle size and loss of the spherical shape in the secondary particles.

Synthesis in DMSO. Because of its particular properties, DMSO has become quite popular as a medium to prepare different nanostructures in colloidal dispersions. Its high dielectric constant, its ability to act as a complexing agent due to its high basic character and its high viscosity, helps to modulate the interface tension, stabilizing nanoparticles at small sizes.[26,65−72]

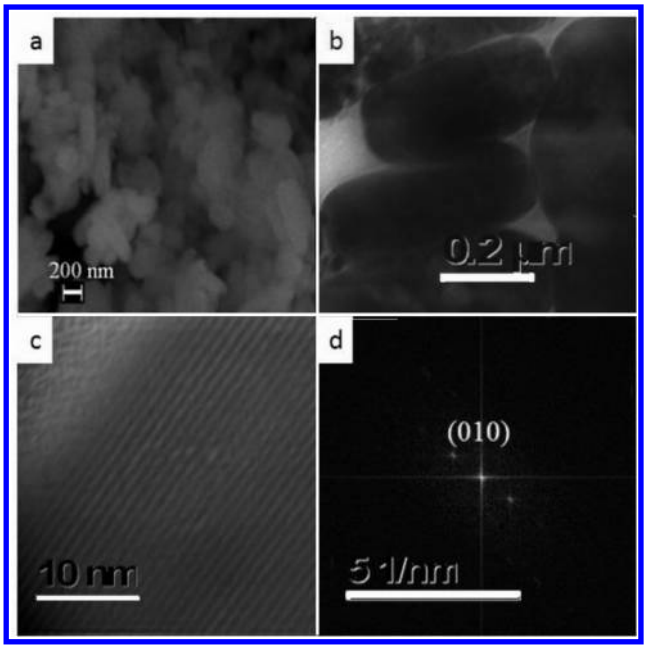

Figure 5. (a) SEM and (b) TEM images of $BaSO_4$ aggregates prepared without EDTA. (c) High-magnification HRTEM image of the $BaSO_4$ clusters. (d) FFT analysis of the HRTEM image.

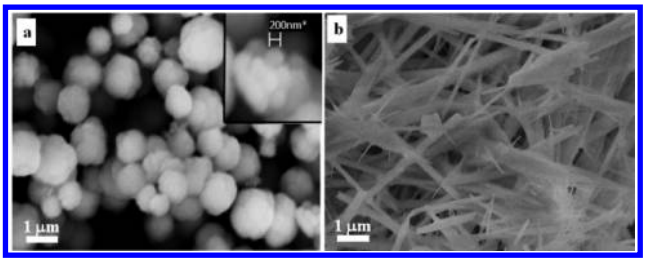

Figure 6. $BaSO_4$ aggregates DMSO/EDTA at room temperature: (a) after the reaction and (b) past 8 days of aging.

(65) Németh, J.; Rodríguez-Gattorno, G.; Díaz, D.; Vázquez-Olmos, A. R.; Dékány, I. *Langmuir* **2004**, *20*, 2855–2860.
(66) Allen, H. C.; Gragson, D. E.; Richmond, G. L. *J. Phys. Chem. B* **1999**, *103*, 660–666.
(67) Mizuno, K.; Imafuji, S.; Ochi, T.; Ohta, T.; Maeda, S. *J. Phys. Chem. B* **2000**, *104*, 11001–11005.
(68) Pál, E.; Dékány, I. *Colloids Surf. A* **2008**, *318*, 141–150.
(69) Patakfalvi, R.; Oszkó, A.; Dékány, I. *Colloids Surf. A* **2003**, *220*, 45–54.
(70) Díaz, D.; Castillo-Blum, S. E.; Alvarez-Fregoso, O.; Rodríguez-Gattorno, G.; Santiago-Jacinto, P.; Rendon, L.; Ortiz-Frade, L.; Leon-Paredes, Y.-J. *J. Phys. Chem. B* **2005**, *109*, 22715–22724.
(71) Rodríguez-Gattorno, G.; Santiago-Jacinto, P.; Rendón-Vázquez, L.; Németh, J.; Dékány, I.; Díaz, D. *J. Phys. Chem. B* **2003**, *107*, 12597–12604.
(72) Velasco-Arias, D.; Díaz, D.; Santiago-Jacinto, P.; Rodríguez-Gattorno, G.; Vázquez-Olmos, A.; Castillo-Blum, S. E. *J. Nanosci. Nanotechnol.* **2008**, *8*, 6389–6397.

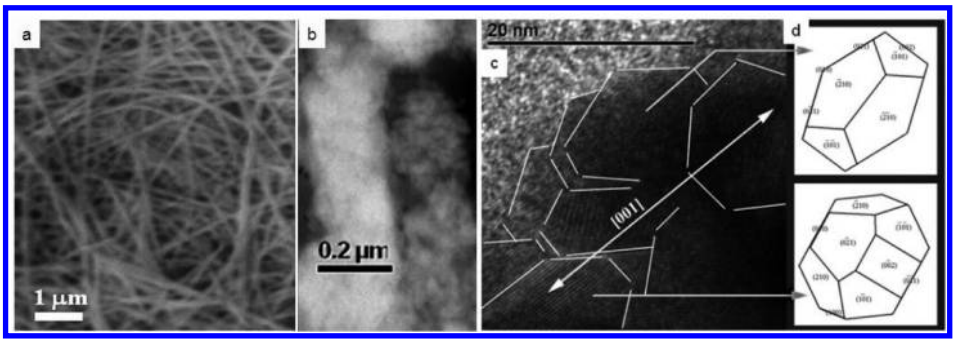

Figure 7. $BaSO_4$ fibers obtained at room temperature in DMSO-EDTA/ (5%) H_2O, after an aging time of 9 days. (a) SEM image, (b) TEM image of $BaSO_4$ aggregates,(c) High-magnification HRTEM image of the $BaSO_4$ clusters, (d) and schematic representation of the estimated morphology (from the SHAPE software).

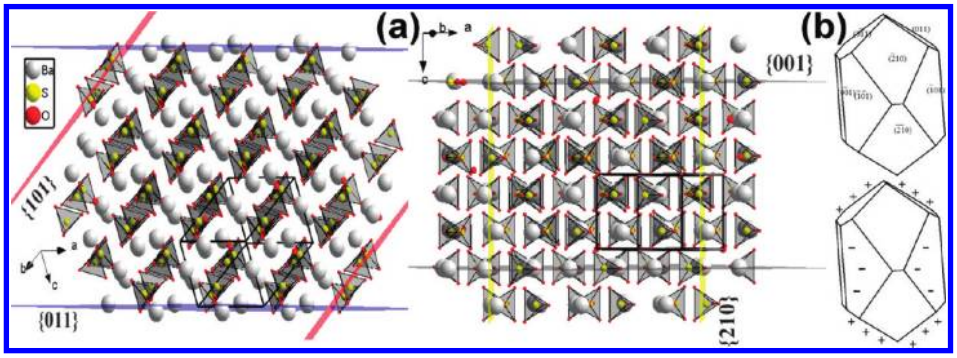

Figure 8. (a) Schematic representation of {101}, {210}, {001}, and {011} plane surfaces in $BaSO_4$. The represented polyhedrons correspond to SO_4^{2-} ions, the light gray balls correspond to Ba^{2+} cations. The structure simulation was carried out using Diamond Software Demo version 3.1 (http://www.crystalimpact.com/diamond/Default.htm) (b) Schematic representations of the $BaSO_4$ nanocrystal surfaces; the plus sign represents those surfaces related only to Ba^{2+}, while the negative sign represents surfaces containing SO_4^{2-}.

A setback is the EDTA low solubility in DMSO that can be overcome by heating at 60 °C.

SEM images of samples synthesized in DMSO/EDTA at 60 °C are shown in Figure 6a. Under these conditions, spherical aggregates with sizes ranging from 500 to 700 nm, composed by primary particles of 200 nm are obtained. These sizes are larger than those obtained in water (see inset in Figure 6a). This is unexpected since the critical nuclei are likely to be smaller in DMSO, due to the lower solubility of $BaSO_4$ in this solvent. To improve EDTA solubility, temperature was increased, and hence the critical nuclei size and growth rate, leading to the increase in particle size. On the other hand, dissociation of EDTA (and, in general, any carboxylated molecule) is also strongly affected when the solvent is changed from water to an organic solvent such as DMSO.[73] Therefore, the role of EDTA as stabilizing agent in organic solvents is offset to a certain extent due to changes in pK_a.

After aging of 8 days, the formation of $BaSO_4$ fibrous aggregates is observed in the SEM images (Figure 6b). The morphology of the fibers is "needle-like" with diameters of ~500 nm. The change in morphology is probably related to a preferential reorganization of the nanoparticles to form an elongated shape. The pH and EDTA solubility, among other factors, affect the morphology. Because of the strong dependence of DMSO properties on water content[74] and the low solubility of EDTA in pure DMSO, we decided to study the influence of small amounts of water in DMSO.

Synthesis in Water (5%)−DMSO in the Presence of EDTA. Figure 7a shows a SEM image of aggregates synthesized in presence of 5 vol % of water and after 9 days of aging. The resulting quasi monodisperse fibers have diameters of less than 200 nm. Dark field images (Figure 7b) show that fibers are formed by aggregates of primary particles. These results suggest that water has a substantial influence during the aging process, favoring the EDTA surface absorption mechanism and allowing the change in morphology from spherical agglomerates to elongated meso-crystal fibers.

HRTEM characterizations elucidate details related to the meso-crystal chemical mechanism that lead to $BaSO_4$ fiber formation. The analysis over several TEM images (e.g.: Figure 7c) indicates that the fibers are composed of several oriented primary particles. The FFT analysis (Supporting Information Figures S2 and S3) performed on nanocrystals, shows that (i) d_{hkl} agrees with reflections expected for $BaSO_4$, (ii) the nanocrystal morphology falls into an orthorhombic−dipyramidal geometry, which is very common in Barite crystals.[33,75] On the basis of measured reflections, it was possible to estimate the nanocrystal orientation, which reveals that fibers form in a kind of hierarchical organization of nanoparticles along the [001] and [010] directions, as shown in Figure 7, parts c and d. Additionally, the most important estimated surfaces, from the HRTEM study were {210}, {001}, {011}, and {101}. These results strongly suggest that organization of particles in elongated fibers follows a brick-like mechanism, where the most important particle−particle interaction take place through {011} and {101} surfaces. Analyzing the modeled structure (see schematic representation in Figure 8) it can be recognized that the {210} and {001} family planes are associated with alternate distributions of Ba^{2+} and

(73) Bordwell, F. G.; Fried, H. E. *J. Org. Chem.* **1981**, *46*, 4327–4331.
(74) Catalan, J.; Díaz, C.; García-Blanco, F. *J. Org. Chem.* **2001**, *66*, 5846–5852.
(75) Radanovic-Guzvica, B. *Geol. Croat.* **1999**, *52*, 59–65.

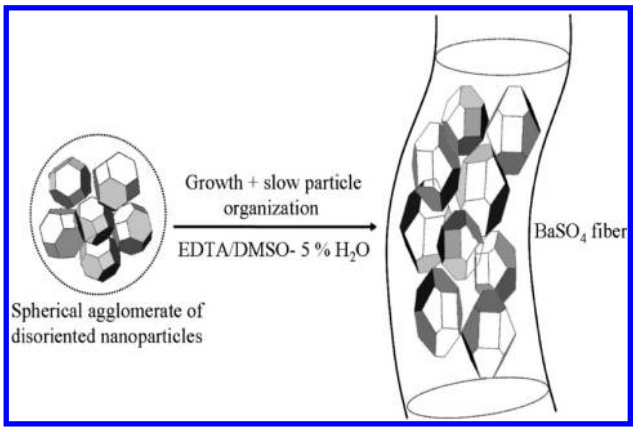

Figure 9. Schematic representation of the fiber formation mechanism by electrostatic multipolar interactions.

SO_4^{2-} along these surfaces, while the {011} and {101} family planes are related exclusively to Ba^{2+} or to SO_4^{2-}, respectively. According to the observed surface distributions from the HRTEM study, it can be envisaged that a preferential EDTA adsorption occurs on those surfaces containing Ba^{2+} (i.e.: the {011} surfaces) while cations (H_3O^+ or Na^+) are expected to be adsorbed on the {101} surfaces. These surfaces are not charge-compensated, since the Ba^{2+} containing surfaces are positively charged (see Figure 8b). It is worth noting that $BaSO_4$ alternates its surface charges deficiencies in such a form that nanoparticle multipoles distribute along the particle as inclined vectors from the center of {011} surfaces toward {101} surfaces. Such an array of dipoles should not have an appreciable net component and particles tend to be randomly oriented in a spherical agglomerate; however this situation is expected to change during aging processes where particle-EDTA interaction change. The EDTA molecule minimizes the particle−particle interactions through the {011} plane surfaces, resulting in a net dipole component, because bonding in Ba−EDTA is stronger and less dissociated than ion−ion interactions on {101} surfaces. Particles organize in brick-like meso-structures, as depicted in Figure 9. This may be a plausible explanation for the preferential spatial organization of the particles into fiber meso-crystals. However, a definitive explanation remains the subject of further research.

Conclusions

The mean particle size, morphology of agglomerates, and secondary particle-size distribution of $BaSO_4$ nanoparticles, obtained from precipitation in solution, strongly depends on reaction conditions. EDTA acts as an efficient capping agent stabilizing very small particles, even in acid pH media where EDTA dissociation is inhibited. The aging processes occurring after few days of preparation slightly modifies the mean particle size, morphology and secondary particle size. However, when DMSO is used as solvent in presence of small amounts of H_2O (5%), long fibers are obtained, resulting from hierarchical organization of $BaSO_4$ nanoparticles. Direct observation of self-assembled primary particles by HRTEM revels that fibers are formed via hierarchical organization of barium sulfate nanoparticles during aging processes. The fibers HRTEM micrographs suggest that this organization occurs preferentially along the (001) and (010) nanoparticle axis via a brick-like mechanism, where EDTA plays an important role in the generation of surface multipolar attractions, leading to the production of elongated fibers.

Acknowledgment. We acknowledge the financial support from PAPIIT-UNAM, project IN103207/20, from Consejo Nacional de Ciencia y Tecnología (CONACyT) through the project 100195. Issis C. Romero-Ibarra acknowledges the financial support of CONACyT under the scholarship register number 181930, and M. F. García-Sánchez acknowledges the ICyT-DF postdoctoral fellowship. The authors acknowledge the work of. Dr. P. S. Schabes-Retchkiman on HRTEM measurements and the technical assistance of L. Baños, A. Tejeda, O. Novelo, J. Camacho, O. Jiménez, T. Vázquez, J. E. Romero-Ibarra, and L. Rendón.

Supporting Information Available: Figures showing XRD of spherical agglomerates and fibers, and FFT analysis performed on the nanocrystals of fibers. This material is available free of charge via the Internet at http://pubs.acs.org.